

A normalized scaled gradient method to solve non-negativity and equality constrained linear inverse problem – Application to spectral mixture analysis

Céline Theys ^{*}, Henri Lantéri ^{*}, Nicolas Dobigeon [†],
Cédric Richard ^{*}, Jean-Yves Tourneret [†] and André Ferrari ^{*}

^{*} Laboratoire Lagrange, Université de Nice Sophia-Antipolis, 06108 Nice

Email: {celine.theys, henri.lanteri, cedric.richard, andre.ferrari}@unice.fr

[†] IRIT/INP-ENSEEIH, Université de Toulouse, 31071 Toulouse Cedex 7, France

Email: {nicolas.dobigeon, jean-yves.tourneret}@enseeiht.fr

Abstract

This paper addresses the problem of minimizing a convex cost function under non-negativity and equality constraints, with the aim of solving the linear unmixing problem encountered in hyperspectral imagery. This problem can be formulated as a linear regression problem whose regression coefficients (abundances) satisfy sum-to-one and positivity constraints. A normalized scaled gradient iterative method (NSGM) is proposed for estimating the abundances of the linear mixing model. The positivity constraint is ensured by the Karush Kuhn Tucker conditions whereas the sum-to-one constraint is fulfilled by introducing normalized variables in the algorithm. The convergence is ensured by a one-dimensional search of the step size. Note that NSGM can be applied to any convex cost function with non negativity and flux constraints. In order to compare the NSGM with the well-known fully constraint least squares (FCLS) algorithm, this latter is reformulated in term of a penalized function, which reveals its suboptimality. Simulations on synthetic data illustrate the performances of the proposed algorithm in comparison with other unmixing algorithms and, more particularly, demonstrate its efficiency when compared to the popular FCLS. Finally, results on real data are given.

I. INTRODUCTION

Hyperspectral and multispectral imagery have received considerable attention in the literature (see for instance [1], [2] and references therein). Hyperspectral and multispectral data are collected in many spectral bands, providing accurate information regarding the observed scene. Recent applications benefiting from multi/hyperspectral imagery include ecosystem monitoring [3], crop measure [4] and natural disaster analysis [5]. Each pixel of such images is represented by a reflectance vector, called spectrum, which contains the measurements associated with the different spectral bands. However, mainly due to the spatial resolution of current spectro-imager, the measured pixel spectrum consists of a mixture of several spectral signatures, usually referred to as *endmembers*, that characterize the macroscopic materials present in this pixel [6], [7]. Identifying these endmembers and estimating their corresponding fractions, or *abundances*, in each image pixel is the core of the linear spectral mixture analysis (LSMA). As a first approximation, it is widely admitted that each pixel of the image can be accurately modeled as a linear mixture of the endmembers. Following this linear mixing model (LMM), LSMA can be addressed following two steps. First, it is important to identify the spectral signatures associated to the endmembers. Very popular algorithms allowing endmember determination are N-FINDR algorithm proposed by Winter [8] and vertex component analysis (VCA) introduced in [9]. The second step within LSMA is the linear unmixing of each pixel of the image. Linear unmixing consists of estimating the abundance of each endmember contained in a given pixel. The linear unmixing problem is challenging because the abundances have to satisfy sum-to-one and positivity constraints.

There are mainly two kinds of approaches which can be used to estimate abundances that satisfy these constraints. The first approach is to define appropriate prior distributions for the abundances (satisfying the sum-to-one and positivity constraints) and estimate the unknown parameters from the resulting joint posterior distribution following the principles of Bayesian inference [10]. However, the complexity of the parameter posterior distribution (essentially due to the constraints inherent to abundances) requires to develop sophisticated sampling algorithms to compute the Bayesian estimators. These algorithms include the Gibbs sampler or the Metropolis-within-Gibbs algorithm [11]. This approach was for instance advocated in [10] and provided interesting results. The price to pay with Bayesian unmixing algorithms is the high computational complexity resulting from the sampling strategy.

The second approach consists of estimating the abundances by minimizing an appropriate

cost function such as the least squares criterion under sum-to-one and positivity constraints. As explained in [12], there is no analytical solution for this optimization problem because of the linear inequalities resulting from the positivity constraints. However, an efficient iterative algorithm referred to as fully constrained least square (FCLS) algorithm has been proposed in [12]. The FCLS has been applied successfully to the unmixing of hyperspectral images. More recently, another algorithm called projected scaled gradient method (PSGM) has been proposed in [13] where the sum-to-one constraint is ensured by a projection at each iteration. An important advantage of the estimators proposed in [12] and [13] is their reduced computational cost, in regard to Bayesian strategy. However, the convergence of these algorithms to the global minimum of the cost function of interest is generally not ensured, which is their main drawback.

This paper studies a normalized split gradient method (NSGM) for estimating the abundances involved within the LMM under positivity and sum-to-one constraints. The convergence of the NSGM is ensured for an appropriate step size, which makes this approach very attractive. In order to compare the proposed NSGM with the popular FCLS algorithm, we will show that in the FCLS algorithm, the flux constraint is ensured by including a penalty term into the quadratic data term. The paper is organized as follows. In Section II, the normalized scaled gradient method is developed to minimize a general criterion under positivity constraints. The problem of taking a flux constraint (i.e., the additivity constraint) into account is addressed in Section III. The resulting iterative algorithm to perform LSMA, i.e., to solve the LMM-based unmixing problem, is derived in Section IV. In Section V, explicit form of the flux constraint is given. Simulation results conducted on synthetic and real data are presented in Section VI. Conclusions are reported in Section VII.

II. SCALED GRADIENT ALGORITHM FOR POSITIVITY CONSTRAINTS

This section studies an iterative method referred to as scaled gradient method (SGM) to minimize any convex criterion under positivity constraints. In other words, first the sum-to-one constraint is not taken into account but it will be handled in the next section. Minimizing a convex cost function J under inequality constraints can be classically achieved by introducing the Lagrange function. The Lagrange function \mathcal{L} associated to the linear unmixing problem with positivity constraints can be written as

$$\mathcal{L}(\boldsymbol{\alpha}, \boldsymbol{\lambda}) = J(\boldsymbol{\alpha}) - \boldsymbol{\lambda}^T \mathbf{g}(\boldsymbol{\alpha}),$$

where $\boldsymbol{\lambda} = [\lambda_1 \dots \lambda_R]^T$ contains the Lagrange multipliers and $\mathbf{g}(\boldsymbol{\alpha}) = (g(\alpha_1) \dots g(\alpha_R))^T$. Let us note that the method proposed hereafter is valid for any differentiable criterion J . Moreover if the criterion is convex and gradient Lipschitz, as in (24), the proposed method converges to the global minimum of the cost function J . The function g has to be chosen to express the positivity constraints. More precisely, g is an increasing function that must be positive for inactive constraints ($\alpha_r > 0$), and zero for active constraints ($\alpha_r = 0$). The Karush Kuhn Tucker (KKT) conditions [14], [15] at the optimum $(\boldsymbol{\alpha}^*, \boldsymbol{\lambda}^*)$ express as follows

$$[\nabla_{\boldsymbol{\alpha}} \mathcal{L}(\boldsymbol{\alpha}^*, \boldsymbol{\lambda}^*)]_r = 0, \quad \forall r, \quad (1)$$

$$g(\alpha_r^*) \geq 0, \quad \forall r, \quad (2)$$

$$\lambda_r^* \geq 0, \quad \forall r, \quad (3)$$

$$\lambda_r^* g(\alpha_r^*) = 0, \quad \forall r, \quad (4)$$

where $\nabla_{\boldsymbol{\alpha}} \mathcal{L}$ is the gradient of \mathcal{L} with respect to (w.r.t.) $\boldsymbol{\alpha}$ and the notation $[\cdot]_r$ is used for the r th component of a vector. As a consequence, (1) leads to

$$\lambda_r^* \frac{\partial g(\alpha_r^*)}{\partial \alpha_r} = [\nabla_{\boldsymbol{\alpha}} J(\boldsymbol{\alpha}^*)]_r.$$

Equivalently, the r th Lagrange multiplier can be computed as

$$\lambda_r^* = \frac{[\nabla_{\boldsymbol{\alpha}} J(\boldsymbol{\alpha}^*)]_r}{\frac{\partial g(\alpha_r^*)}{\partial \alpha_r}}, \quad r = 1, \dots, R.$$

Taking into account the properties of g , (4) reduces to:

$$[\nabla_{\boldsymbol{\alpha}} J(\boldsymbol{\alpha}^*)]_r g(\alpha_r^*) = 0, \quad r = 1, \dots, R. \quad (5)$$

This last equation allows an iterative algorithm to be derived to estimate $\boldsymbol{\alpha}$ under positivity constraints.

Let us note that the choice for g can lead to some properties on the algorithm speed. For example, taking a power function with an exponent smaller than 1 accelerates the algorithm (see Appendix A). If the descent step-size is computed to monitor the convergence of the algorithm, an obvious choice for $g(\cdot)$ is $g(\alpha_r) = \alpha_r$. Then, more generally, the r th component of the descent direction can be

$$f_r(\boldsymbol{\alpha}) \hat{\alpha}_r [-\nabla_{\boldsymbol{\alpha}} J(\hat{\boldsymbol{\alpha}})]_r \quad (6)$$

where $f_r(\boldsymbol{\alpha})$ is a positive function scaling the gradient, leading to the scaled gradient method (SGM)

$$\alpha_r^{(k+1)} = \alpha_r^{(k)} + \gamma_r^{(k)} f_r(\boldsymbol{\alpha}^{(k)}) \alpha_r^{(k)} [-\nabla_{\boldsymbol{\alpha}} J(\boldsymbol{\alpha}^{(k)})]_r, \quad (7)$$

where $\gamma_r^{(k)}$ is the descent step-size that must be adjusted to ensure convergence of the algorithm.

An interesting choice for the scaling function $f_r(\cdot)$ initially proposed in [16] is recalled below. The negative gradient of any convex cost function $J(\alpha)$ with a finite minimum can always be expressed as the difference between two positive functions:

$$- [\nabla_{\alpha} J(\alpha^{(k)})]_r = [U(\alpha^{(k)})]_r - [V(\alpha^{(k)})]_r. \quad (8)$$

By choosing the scaling function as

$$f_r(\alpha^{(k)}) = \frac{1}{[V(\alpha^{(k)})]_r}, \quad (9)$$

then equation (7) becomes:

$$\alpha_r^{(k+1)} = \alpha_r^{(k)} + \gamma_r^{(k)} \alpha_r^k \left(\frac{[U(\alpha^{(k)})]_r - [V(\alpha^{(k)})]_r}{[V(\alpha^{(k)})]_r} \right). \quad (10)$$

Let us determine the maximum value for the step size in order that $\alpha_r^{(k+1)} \geq 0$, given $\alpha_r^{(k)} \geq 0$. Note that, according to (10), a restriction may only apply for the set of index r such that

$$[U(\alpha^{(k)})]_r - [V(\alpha^{(k)})]_r < 0 \quad (11)$$

since the other terms are positive. The maximum step size which ensures the positivity of $\alpha_r^{(k+1)} \geq 0$ is given by

$$(\gamma_r^k)_{\max} = \left[1 - \frac{[U(\alpha^{(k)})]_r}{[V(\alpha^{(k)})]_r} \right]^{-1} \quad (12)$$

which is strictly greater than 1. Finally, the maximum step size over all the components must satisfy

$$\gamma_{\max}^k \leq \min_r \{(\gamma_r^k)_{\max}\}. \quad (13)$$

This choice ensures the non-negativity of the components of $\alpha_r^{(k)}$ from iteration to iteration.

We can then write the algorithm (10) with a step size γ independent of the component

$$\alpha_r^{(k+1)} = \alpha_r^{(k)} + \gamma^{(k)} \alpha_r^k \left(\frac{[U(\alpha^{(k)})]_r - [V(\alpha^{(k)})]_r}{[V(\alpha^{(k)})]_r} \right). \quad (14)$$

The step size ensuring the convergence of the algorithm must be computed by an economic line search, i.e, following the Armijo rule (see appendix B), searched in the range $]0, \gamma_{\max}^k[$.

The step size can be chosen equal to 1, $\gamma_r^{(k)} = 1, \forall r = 1, \dots, R$, then, we obtain the classical multiplicative algorithm:

$$\alpha_r^{(k+1)} = \alpha_r^{(k)} \frac{[U(\alpha^{(k)})]_r}{[V(\alpha^{(k)})]_r}.$$

This multiplicative form is very attractive since the positivity of $\alpha_r^{(k)}$ throughout the algorithm iterations is ensured for any positive initial value $\alpha_r^{(0)}$ positive but the convergence is not ensured in the general case. However, in some particular cases, for instance if $J(\hat{\alpha})$ is a quadratic cost function, we obtain the iterative space reconstruction algorithm (ISRA) algorithm whose convergence has been proved in [17].

III. ALGORITHMS FOR POSITIVITY AND SUM-TO-ONE CONSTRAINTS

A. Normalized SGM

In the case where parameters are subject to positivity and sum-to-one constraints, we propose a normalized SGM (NSGM) by introducing the non-normalized variable $\mathbf{u} = [u_1 \dots u_R]^T$ related to α by

$$\alpha = \frac{\mathbf{u}}{\sum_j u_j}. \quad (15)$$

Let us note that if $\sum_j u_j$ is a constant and if J is convex w.r.t. α , then J is also convex w.r.t. \mathbf{u} . This property will be important in the following.

The gradient of J w.r.t. a component u_r is

$$\frac{\partial J}{\partial u_r} = \sum_{l=1}^R \frac{\partial J}{\partial \alpha_l} \frac{\partial \alpha_l}{\partial u_r}, \quad (16)$$

hence

$$\frac{\partial J}{\partial u_r} = \frac{1}{\sum_j u_j} \left(\frac{\partial J}{\partial \alpha_r} - \sum_{l=1}^R \alpha_l \left(\frac{\partial J}{\partial \alpha_l} \right) \right). \quad (17)$$

Thus the negative gradient of J can be decomposed as in (8) with

$$[U(\mathbf{u}^{(k)})]_r = \frac{1}{\sum_j u_j^{(k)}} \left(\frac{-\partial J}{\partial \alpha_r} - \min_r \left(-\frac{\partial J}{\partial \alpha_r} \right) + \epsilon \right), \quad (18)$$

$$[V(\mathbf{u}^{(k)})]_r = \frac{1}{\sum_j u_j^{(k)}} \left(\sum_{l=1}^R \alpha_l \left(\frac{-\partial J}{\partial \alpha_l} \right) - \min_r \left(-\frac{\partial J}{\partial \alpha_r} \right) + \epsilon \right). \quad (19)$$

Note that the term $\min_r \left(-\frac{\partial J}{\partial \alpha_r} \right)$ is subtracted to ensure positivity of both U and V whereas ϵ is a small fixed constant, that does not modify the gradient but avoid the division by zero in (14). Then the final algorithm based on (10) with the particular choice for $f(\cdot)$ given by (9) and expressions (18), (19) is:

$$u_r^{(k+1)} = u_r^{(k)} + \gamma_r^{(k)} u_r^{(k)} \left(\frac{\frac{-\partial J}{\partial \alpha_r} - \min_r \left(-\frac{\partial J}{\partial \alpha_r} \right) + \epsilon}{\sum_{l=1}^R \alpha_l \left(\frac{-\partial J}{\partial \alpha_l} \right) - \min_r \left(-\frac{\partial J}{\partial \alpha_r} \right) + \epsilon} - 1 \right). \quad (20)$$

It can be easily found that the flux is maintained on \mathbf{u} , i.e.,

$$\sum_j u_j^{(k+1)} = \sum_j u_j^{(k)}. \quad (21)$$

As noticed above, the convexity of J w.r.t. α is ensured. This allows us to come back to the initial variables α , finally leading to the following updating rule of the proposed NSGM

$$\alpha_r^{(k+1)} = \alpha_r^{(k)} + \gamma_r^{(k)} \alpha_r^{(k)} \left(\frac{\frac{-\partial J}{\partial \alpha_r} - \min_r \left(-\frac{\partial J}{\partial \alpha_r} \right) + \epsilon}{\sum_{l=1}^R \alpha_l \left(\frac{-\partial J}{\partial \alpha_l} \right) - \min_r \left(-\frac{\partial J}{\partial \alpha_r} \right) + \epsilon} - 1 \right). \quad (22)$$

The step sizes $\gamma_r^{(k)}$ are tuned following the Armijo rule [18] (see Appendix B), at each iteration k , to ensure the convergence of the algorithm.

One can be easily shown that the KKT conditions (1), (2), (3) and (4) are fulfilled at the solution:

- If the solution $\alpha_r^* > 0$, then from (7), $[-\nabla_{\alpha} J(\alpha^*)]_r = 0$.
- If $\alpha_r^* = 0$ and $[\nabla_{\alpha} J(\alpha^*)]_r < 0$, there is a contradiction because the term $(1 + \gamma_r^{(k)} f_r(\alpha^{(k)})) [-\nabla_{\alpha} J(\alpha^{(k)})]_r$ is greater than 1 in the neighborhood of α_r^* and the solution will never be reached.

IV. APPLICATION TO LSMA

Within a widely admitted LSMA framework, the LMM assumes that a mixed pixel \mathbf{y} resulting from an observation in L spectral bands can be written as a linear combination of R endmember spectra $\mathbf{M}_1, \dots, \mathbf{M}_R$

$$\mathbf{y} = \mathbf{M}\alpha + \mathbf{e} \quad (23)$$

where $\mathbf{M} = (\mathbf{M}_1 \dots \mathbf{M}_R)$ is the $L \times R$ matrix of the endmember spectra, $\alpha = (\alpha_1 \dots \alpha_R)^T$ is the abundance vector to be estimated and \mathbf{e} is an additive noise. The linear unmixing problem considered in this paper consists of estimating α under positivity and sum-to-one constraints

$$\alpha_r \geq 0, \forall r = 1, \dots, R \text{ and } \sum_{r=1}^R \alpha_r = 1.$$

A standard assumption related to the LMM defined in (23) is that the noise vector is distributed according to a Gaussian distribution with zero-mean and covariance matrix $\Sigma = \sigma^2 \mathbf{I}_L$, where \mathbf{I}_L is the $L \times L$ identity matrix. Note that this statistical model assumes that the noise variance is the same in all bands. This assumption has been used extensively in the literature (see for instance [19], [20], [21]). Since the variance σ^2 can be easily estimated

from the observation vector, it is assumed to be known in this paper. After removing the additive and multiplicative constants, the resulting negative log-likelihood function associated to the observed model reduces to the following cost function

$$J(\boldsymbol{\alpha}) = \frac{1}{2}(\mathbf{y} - \mathbf{M}\boldsymbol{\alpha})^T(\mathbf{y} - \mathbf{M}\boldsymbol{\alpha}). \quad (24)$$

The opposite of the gradient is then

$$\frac{\partial J}{\partial \alpha_r} = \mathbf{M}^T \mathbf{y} - \mathbf{M}^T \mathbf{M} \boldsymbol{\alpha} \quad (25)$$

and the resulting iterative algorithm on $\boldsymbol{\alpha}$ to conduct LSMA is given by the following updating rule

$$\alpha_r^{(k+1)} = \alpha_r^{(k)} + \gamma_r^{(k)} \alpha_r^{(k)} \left(\frac{\frac{-\partial J}{\partial \alpha_r} - \min_r \left(-\frac{\partial J}{\partial \alpha_r} \right) + \epsilon}{\sum_{l=1}^R \alpha_l \left(\frac{-\partial J}{\partial \alpha_l} \right) - \min_r \left(-\frac{\partial J}{\partial \alpha_r} \right) + \epsilon} - 1 \right). \quad (26)$$

V. INTERPRETATION OF THE FCLS ALGORITHM

The FCLS algorithm [12] is popular tool to solve the linear unmixing problem detailed in section IV, briefly recalled below

$$\min_{\boldsymbol{\alpha}} (\mathbf{y} - \mathbf{M}\boldsymbol{\alpha})^T(\mathbf{y} - \mathbf{M}\boldsymbol{\alpha}) \quad (27)$$

with

$$\alpha_r \geq 0, \forall r = 1, \dots, R \text{ and } \sum_{r=1}^R \alpha_r = 1.$$

Within the FCLS scheme, the positivity constraint is ensured using the nonnegative least squares (NNLS) method, proposed by Lawson and Hanson [22]. Regarding the sum-to-one constraint, Heinz and Chang introduce in [12] a new signature matrix \mathbf{N} and a new observation vector \mathbf{s} defined by

$$\mathbf{N} = \begin{bmatrix} \delta \mathbf{M} \\ \mathbf{1}^T \end{bmatrix} \quad \text{and} \quad \mathbf{s} = \begin{bmatrix} \delta \mathbf{y} \\ 1 \end{bmatrix}, \quad (28)$$

with $\mathbf{1} = (1 \dots 1_R)^T$. The initial unmixing problem then becomes

$$\min_{\boldsymbol{\alpha}} (\mathbf{s} - \mathbf{N}\boldsymbol{\alpha})^T(\mathbf{s} - \mathbf{N}\boldsymbol{\alpha}) \quad (29)$$

with

$$\alpha_r \geq 0, \forall r = 1, \dots, R.$$

The negative gradient w.r.t. α is then

$$-\nabla_{\alpha} J(\alpha) = \mathbf{N}^T \mathbf{s} - \mathbf{N}^T \mathbf{N} \alpha, \quad (30)$$

$$= \delta^2 M^T \mathbf{y} + 1 - \delta^2 M^T M \alpha - \sum_i \alpha_i, \quad (31)$$

$$= M^T \mathbf{y} - M^T M \alpha + \frac{1}{\delta^2} - \frac{1}{\delta^2} \sum_i \alpha_i. \quad (32)$$

Note that (30) corresponds to the negative gradient of:

$$J(\alpha) = (\mathbf{y} - M\alpha)^T (\mathbf{y} - M\alpha) + \frac{1}{2\delta^2} \left(\sum_i \alpha_i - 1 \right)^2. \quad (33)$$

This result shows that the sum-to-one constraint is taken into account within the FCLS algorithm by adding a penalization to the data fidelity term. Consequently, the flux conservation is not ensured at each iteration and only in an approximate way at the convergence. Moreover it depends on the regularization parameter $1/2\delta^2$ that needs to be empirically tuned. To conclude, the fundamental difference with the proposed NSGM lies in the fact that we propose an interior point method: at each iterative step, the current estimates satisfy all the constraints and we search for the best estimate among the proposed solutions.

VI. SIMULATION RESULTS

A. Synthetic data

Many simulations have been conducted to validate the previous NSGM algorithm in the LSMA context. The first experiment has been conducted on a linear mixture of $R = 3$ endmembers with $\alpha = [0.3, 0.6, 0.1]^T$. The Armijo rule has been implemented with parameters $\beta = \frac{1}{2}$ and $\sigma = \frac{1}{4}$. The three endmembers used in this example have been extracted from the ENVI library [23] and correspond to the spectra of the construction concrete, green grass and micaceous loam. The NSGM defined by (26) has been applied on these simulated data corrupted by an additive Gaussian noise with a signal-to-noise ratio $\text{SNR} = 25\text{dB}$. Figure 1 shows a typical example of abundance estimates $\alpha^{(k)}$ as a function of the number of iterations k . The algorithm clearly converges after very few iterations.

The means of the estimated abundances with NSGM averaged over 100 Monte Carlo runs are depicted in Figure 2 as a function of the SNR and compared to those obtained with the FCLS algorithm [12], the Bayes estimator [10], the SGM algorithm (without flux constraint) detailed in Section II and the PSGM algorithm [13]. The corresponding estimate variances are given in separate tables, namely Tables I, II and III for parameters α_1 , α_2 and α_3 , respectively.

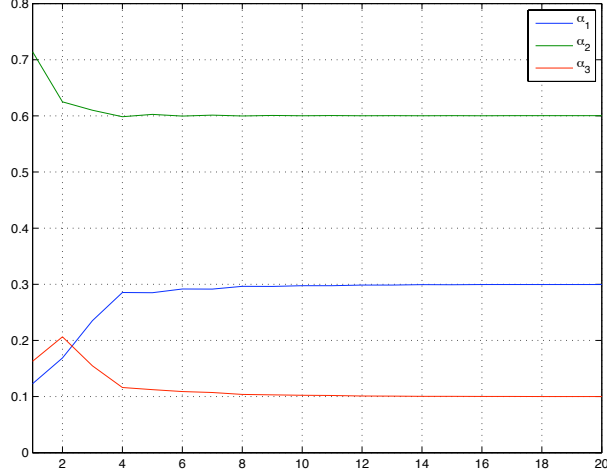


Fig. 1. Typical NSGM estimate $\alpha^{(k)}$ of the abundance vector α versus the iteration number k for $\text{SNR} = 25\text{dB}$.

TABLE I
VARIANCE OF α_1 AS A FUNCTION OF THE SNR

SNR(dB)	-10	0	10	20
Bayes	$1.3e^{-2}$	$6.0e^{-3}$	$1.6e^{-3}$	$1.5e^{-4}$
FCLS	$4.8e^{-2}$	$1.2e^{-2}$	$1.4e^{-3}$	$1.4e^{-4}$
SGM	$5.7e^{-2}$	$9.5e^{-3}$	$1.0e^{-3}$	$1.0e^{-4}$
PSGM	$5.8e^{-2}$	$8.7e^{-3}$	$1.0e^{-3}$	$1.0e^{-4}$
NSGM	$5.8e^{-2}$	$8.2e^{-3}$	$1.0e^{-3}$	$1.0e^{-4}$

Fig. 3 shows the means and the standard deviations of the estimated abundances for both FCLS and NSGM. Initial values of the abundances have been uniformly drawn in the domain defined by the constraints for each Monte Carlo run. Figure 2 shows that the means obtained with the five algorithms are very similar for a SNR level over 10dB . However, for low SNR, the iterative algorithms SGM, PSGM and NSGM perform better. Note also that their performances are very similar. However, in the case of SGM, the sum over the components of α fluctuates around *one* without summing exactly to one. Moreover, the convergence of PSGM is not ensured contrary to the proposed NSGM. Figure 3 shows that the performances of FCLS and NSGM are very similar in terms of mean and variance of the estimates but, again, the flux constraint is strictly imposed only in the case of NSGM as it has been demonstrated in Section V.

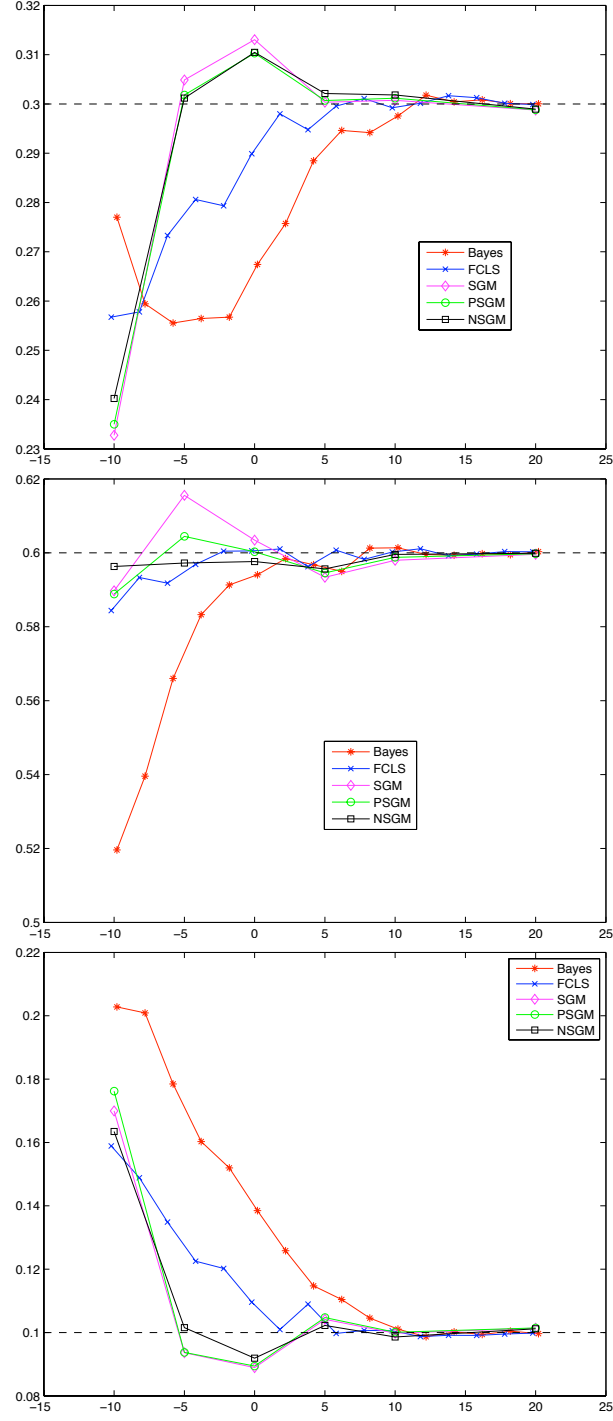


Fig. 2. Means of the abundances versus SNR for 100 noise realizations

B. Real AVIRIS data

The proposed unmixing algorithm has been also applied on two real hyperspectral images acquired by the JPL spectroimager AVIRIS, the Cuprite mining site (NV, USA) and the

TABLE II
VARIANCE OF α_2 AS A FUNCTION OF THE SNR

SNR(dB)	-10	0	10	20
Bayes	$2.1e^{-2}$	$4.1e^{-3}$	$4e^{-4}$	$4e^{-5}$
FCLS	$3.5e^{-2}$	$4.2e^{-3}$	$4e^{-4}$	$4e^{-5}$
SGM	$6.6e^{-2}$	$5.1e^{-3}$	$5e^{-4}$	$5e^{-5}$
PSGM	$5.4e^{-2}$	$4.7e^{-3}$	$3e^{-4}$	$4e^{-5}$
NSGM	$4.8e^{-2}$	$5.3e^{-3}$	$2e^{-4}$	$3e^{-5}$

TABLE III
VARIANCE OF α_3 AS A FUNCTION OF THE SNR

SNR(dB)	-10	0	10	20
Bayes	$7.7e^{-3}$	$3.3e^{-3}$	$1.1e^{-3}$	$1e^{-4}$
FCLS	$34.0e^{-3}$	$8.4e^{-3}$	$1.0e^{-3}$	$1e^{-4}$
SGM	$34.6e^{-3}$	$5.0e^{-3}$	$0.9e^{-3}$	$1e^{-4}$
PSGM	$37.9e^{-3}$	$5.3e^{-3}$	$0.9e^{-3}$	$1e^{-4}$
NSGM	$33.0e^{-3}$	$4.5e^{-3}$	$0.8e^{-3}$	$1e^{-4}$

Purdue Indiana Indian test site (IN, USA).

1) *Cuprite*: This dataset has received considerable attention in the literature since geologic characteristics of the scene have been mapped in [24], [25]. The sample analyzed in this experiment consists of a sub-image of 190×250 that has been initially studied in [9]. Following the choice in [9], $R = 14$ endmember spectra have been extracted by the vertex component analysis (VCA) [9]. Then, the proposed unmixing procedure has been applied pixel-by-pixel to evaluate the relative contribution of each endmember in each image pixel. The abundance maps are depicted in Fig. 4 where a black (resp. white) pixels correspond to absence (resp. presence) of the corresponding endmembers. Note that several areas with dominant endmembers are clearly recovered as similar to those identified in [9].

2) *Indian Pines*: The use of the abundances as features to classify the voxels of hyper-spectral image is today a well established approach (see for example [26]). It relies on both the dimensionality reduction and the physical meaningful of the abundance vector.

The gain provided by the proposed unmixing algorithm in a classification framework has been evaluated on the Indian Pines data. Figure 5 shows a typical spectral band of the

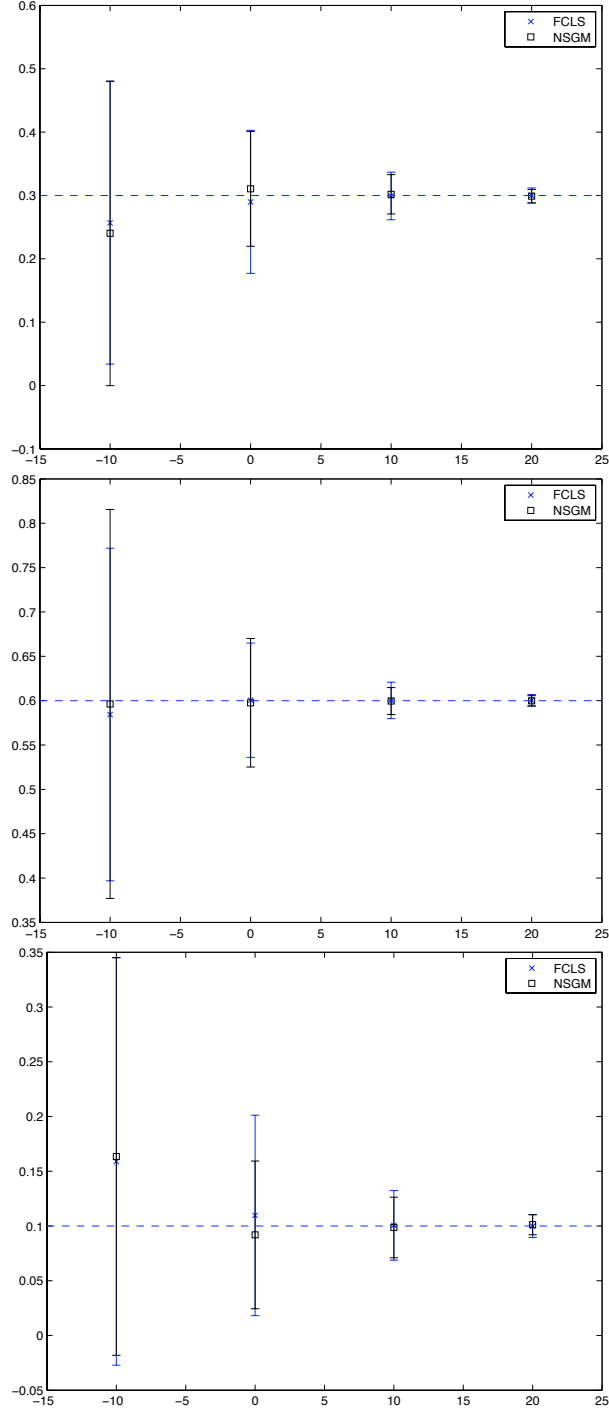


Fig. 3. Means and variances of the abundances versus SNR for FCLS and NSGM

$145 \times 145 \times 200$ data cube. The ground truth image shown in Figure 6(a) reveals 16 distinct object classes and an additional background class.

The procedure followed to assess the performance of the unmixing algorithms is detailed

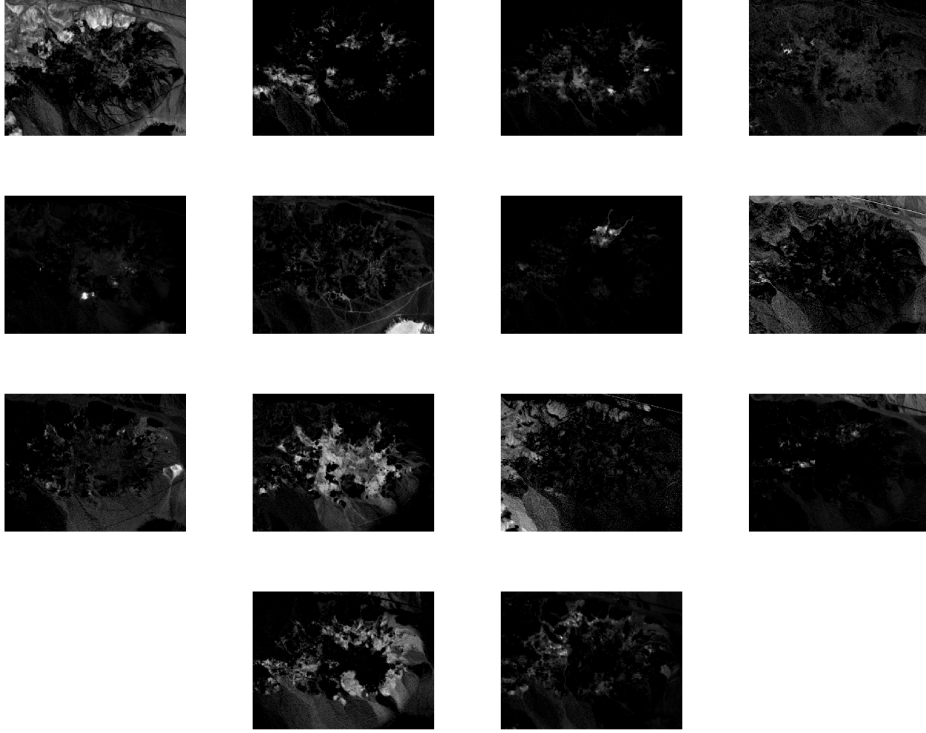


Fig. 4. Abundance maps estimated by the proposed normalized SGM.

in what follows. First, a principal component analysis has been conducted to reduce the dimensionality of the image. The spectra have been projected on the subspace spanned by the 40 principal components, the resulting data cube containing approximately 99% of the total cube power. Then $R = 18$ endmembers (16 corresponding to the number of classes in the ground truth, plus 2 additional for the background class), have been extracted using VCA. Finally, abundances have been estimated with the FCLS algorithm [12], the SUNSAL algorithm [27] and the proposed fully constrained method, NSGM.

Classification of the abundances has been performed using the support-vector-machine multi-classes one-against-all algorithm, [28]. The kernel is chosen as Gaussian with bandwidth equal to 3 and the regularization parameter is set to 10^{-7} . The classifier has been trained using 10% of the abundances of each class. Figure 6 shows a significative result of the classification obtained by the considered methods. Note that for this particular choice of

training data 63.23% of voxels are correctly classified with FCLS, 63.05% with SUNSAL and 64.14% with NSGM. A Monte Carlo simulation has been performed using 100 different training sets randomly chosen in the image. The mean number of correctly classified voxels is 61.3% for FCLS, 61.7 for SUNSAL and 62.3% for NSGM. In this context of classification, the advantage of the proposed method can be explained by the fact that, contrary to FCLS and SUNSAL, NSGM estimates abundances that strictly complies to the constraints.

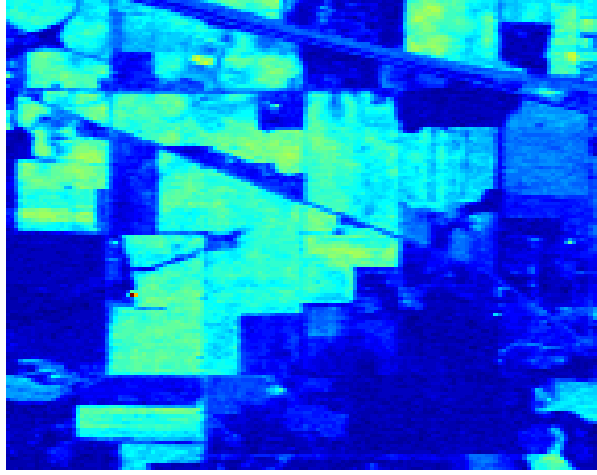


Fig. 5. Indian Pines data. Image at wavelength #186.

VII. CONCLUSIONS

Constrained scaled gradient methods were initially derived for linear models subjected to positivity constraints. This paper studied a normalized scaled gradient method (NSGM) with positivity and sum-to-one constraints. NSGM can be applied to any differentiable criterion contrary to previous proposed algorithm, all the constraints being fulfilled at each iteration (characteristic to interior points methods), with an ensured convergence. The efficiency of the proposed NSGM was illustrated in a LSMA context for the estimation of abundances. The results obtained on synthetic and real data were very promising.

APPENDIX

A. Discussion on the relation between the function g and the algorithm speed

In Section II, the non-negativity constraint is expressed using the function $g(\alpha) = \alpha$. This appendix shows that other functions can be used, resulting in other multiplicative algorithms

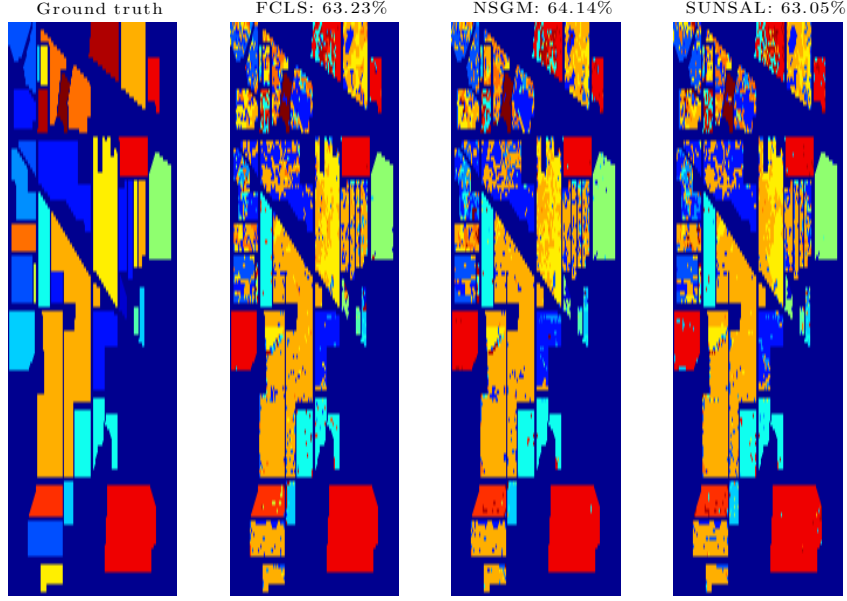


Fig. 6. Indian pines classification. Fig. (a): Ground truth. Fig. (b): Classification result using FCLS unmixing. 63.23% of voxels are correctly classified. Fig. (c): Classification result using NSGM unmixing. 64.14% of voxels are correctly classified. Fig. (d): Classification result using SUNSAL. 63.05% of voxels are correctly classified.

with higher convergence rates. Let us consider, for example, the case where the non-negativity constraint is expressed using the general function $g(\alpha) = \alpha^{1/n}$, with $n \in \mathcal{N}^*$. Taking the decomposition (8):

$$- [\nabla_{\alpha} J(\alpha^{(k)})]_r = [U(\alpha^{(k)})]_r - [V(\alpha^{(k)})]_r. \quad (34)$$

The KKT condition (30) writes at the solution

$$\alpha_r^{1/n} ([U(\alpha)]_r - [V(\alpha)]_r) = 0 \quad (35)$$

that can be modified in the equivalent form

$$\frac{\alpha_r}{[V(\alpha)]_r^n} ([U(\alpha)]_r^n - [V(\alpha)]_r^n). \quad (36)$$

The expression

$$\frac{([U(\alpha)]_r^n - [V(\alpha)]_r^n)}{[V(\alpha)]_r^n} \quad (37)$$

can be expanded in the form

$$\frac{([U(\alpha)]_r - [V(\alpha)]_r)}{[V(\alpha)]_r} \left[1 + \sum_{p=0}^{n-1} [V(\alpha)]_r^{p-n+1} [U(\alpha)]_r^{n-1-p} \right]. \quad (38)$$

Then the algorithm can be rewritten in the form

$$\alpha_r^{(k+1)} = \alpha_r^{(k)} + \gamma_r^{(k)} \alpha_r \frac{([U(\alpha)]_r - [V(\alpha)]_r)}{[V(\alpha)]_r} \left[1 + \sum_{p=0}^{n-1} [V(\alpha)]_r^{p-n+1} [U(\alpha)]_r^{n-1-p} \right]. \quad (39)$$

The function $f_r(\alpha)$ is then

$$f_r(\alpha) = \frac{1}{[V(\alpha)]_r} \left[1 + \sum_{p=0}^{n-1} [V(\alpha)]_r^{p-n+1} [U(\alpha)]_r^{n-1-p} \right]. \quad (40)$$

The effect of this function consists of a modification of the direction and of the modulus of the descent vector. It is always greater than $1/V$ and when U tends to V , i.e, close to the convergence, it tends to n/V . Then taking a function $g(\alpha) = \alpha^{1/n}$ with $n > 1$ has the effect to multiply the descent step-size by a factor greater than 1 and equal to n close to the convergence. The search of the maximum step size that ensures the non-negativity of the component α follows the same procedure that for $n = 1$ and its value is equal to

$$(\gamma_r^k)_{\max} = \frac{1}{1 - \frac{[U(\alpha^{(k)})]_r^n}{[V(\alpha^{(k)})]_r^n}}. \quad (41)$$

for r such that $[\nabla_{\alpha} J(\alpha)]_r > 0$. It is always greater than one and in the same way, we can obtain a multiplicative form of the algorithm by using a constant stepsize equal to one and in this case the actualization of α is given by

$$\alpha_r^{(k+1)} = \alpha_r^{(k)} \frac{[U(\alpha^{(k)})]_r^n}{[V(\alpha^{(k)})]_r^n}.$$

Clearly, in this case, the use of the exponent $1/n$ proposed in the literature [29], [30] plays the role of an accelerating term but the convergence is not ensured. Let us note that if $0 < n \leq 1$, we can easily show that

$$\frac{[U(\alpha^{(k)})]_r^n - [V(\alpha^{(k)})]_r^n}{[V(\alpha^{(k)})]_r^n} = \frac{[U(\alpha^{(k)})]_r - [V(\alpha^{(k)})]_r}{[V(\alpha^{(k)})]_r} \left(\frac{1}{1 + \left(\frac{[U(\alpha^{(k)})]_r}{[V(\alpha^{(k)})]_r} \right)^n + \left(\frac{[U(\alpha^{(k)})]_r}{[V(\alpha^{(k)})]_r} \right)^{2n} + \dots + \left(\frac{[U(\alpha^{(k)})]_r}{[V(\alpha^{(k)})]_r} \right)^{(n-1)n}} \right) \quad (42)$$

Then taking a function $g(\alpha) = \alpha^{1/n}$ with $0 \leq n \leq 1$ has the effect to multiply the descent step size by a factor smaller than one and consequently to decrease the algorithm speed.

B. Line search and Armijo rule

A line search method consists, at each iteration k , of choosing a descent direction \mathbf{p}^k and a step length γ^k to compute

$$\mathbf{u}^{k+1} = \mathbf{u}^k + \gamma^k \mathbf{p}^k \quad (43)$$

to solve the optimization problem

$$\min_{\mathbf{x} \in \mathbb{R}^n} f(\mathbf{u}) \quad (44)$$

with the following assumptions on $f(\mathbf{u})$:

- $f(\mathbf{u})$ is a convex function with a finite minimum.
- The gradient of $f(\mathbf{u})$ denoted as $\nabla f(\mathbf{u})$, is Lipschitz continuous.

Armijo rule

- Set scalars, $s^k, \beta, L > 0, \mu$ and σ as follows

-

$$s^k = \frac{-\nabla f(\mathbf{u}^k)^T \mathbf{p}^k}{L \|\mathbf{p}^k\|^2} \quad (45)$$

- $\beta \in (0, 1)$
- $\sigma \in (0, \frac{1}{2})$
- Then let γ^k be the largest γ in $\{s^k, \beta s^k, \beta^2 s^k, \dots\}$ such that

$$f(\mathbf{u}^k + \gamma \mathbf{p}^k) - f(\mathbf{u}^k) \leq \sigma \gamma \nabla f(\mathbf{u}^k)^T \mathbf{p}^k \quad (46)$$

Theorem 1: Let the sequence $\{\mathbf{u}\}$ be generated by $\mathbf{u}^{k+1} = \mathbf{u}^k + \gamma^k \mathbf{p}^k$ where \mathbf{p}^k is gradient related and \mathbf{u}^k is chosen by Armijo rule. Then every limit point of the sequence $\{\mathbf{u}\}$ is a stationary point.

REFERENCES

- [1] D. A. Landgrebe, *Signal Theory Methods in Multispectral Remote Sensing*. New York: Wiley, 2003.
- [2] C. I. Chang, *Hyperspectral Imaging: Techniques for Spectral Detection and Classification*. New York: Plenum Publishing Co., 2003.
- [3] G. P. Asner, D. E. Knapp, T. Kennedy-Bowdoin, M. O. Jones, R. E. Martin, J. Boardman, and C. B. Field, “Carnegie airborne observatory: in-flight fusion of hyperspectral imaging and waveform light detection and ranging for three-dimensional studies of ecosystems,” *J. Appl. Remote Sensing*, vol. 1, no. 1, p. 013536, June 2007.
- [4] A. Larsolle and H. Hamid Muhammed, “Measuring crop status using multivariate analysis of hyperspectral field reflectance with application to disease severity and plant density,” *Precision Agriculture*, vol. 8, no. 1–2, pp. 37–47, 2007.
- [5] R. F. Kokalya, B. W. Rockwella, S. L. Haireb, and T. V. V. Kinga, “Characterization of post-fire surface cover, soils, and burn severity at the Cerro Grande Fire, New Mexico, using hyperspectral and multispectral remote sensing,” *Remote Sensing of Environment*, vol. 106, no. 3, pp. 305–325, Feb. 2007.
- [6] N. Keshava and J. F. Mustard, “Spectral unmixing,” *IEEE Signal Processing Magazine*, vol. 19, no. 1, pp. 44–57, Jan. 2002.
- [7] J. M. Bioucas-Dias, A. Plaza, N. Dobigeon, M. Parente, Q. Du, P. Gader, and J. Chanussot, “Hyperspectral unmixing overview: Geometrical, statistical, and sparse regression-based approaches,” *IEEE J. Sel. Topics Appl. Earth Observations and Remote Sens.*, vol. 5, no. 2, pp. 354–379, April 2012.
- [8] M. E. Winter, “Fast autonomous spectral end-member determination in hyperspectral data,” in *Proc. 13th Int. Conf. on Applied Geologic Remote Sensing*, vol. 2, Vancouver, April 1999, pp. 337–344.
- [9] J. M. Nascimento and J. M. Bioucas-Dias, “Vertex component analysis: A fast algorithm to unmix hyperspectral data,” *IEEE Trans. Geosci. and Remote Sensing*, vol. 43, no. 4, pp. 898–910, April 2005.
- [10] N. Dobigeon, J.-Y. Tournet, and C.-I Chang, “Semi-supervised linear spectral unmixing using a hierarchical Bayesian model for hyperspectral imagery,” *IEEE Trans. Signal Process.*, vol. 56, no. 7, pp. 2684–2695, July 2008.
- [11] C. P. Robert and G. Casella, *Monte Carlo Statistical Methods*, ser. Springer Texts in Statistics. New York: Springer-Verlag, 2005.
- [12] D. C. Heinz and C.-I Chang, “Fully constrained least squares linear spectral mixture analysis method for material quantification in hyperspectral imagery,” *IEEE Trans. Geosci. and Remote Sensing*, vol. 39, no. 3, pp. 529–545, March 2001.
- [13] C. Theys, N. Dobigeon, J.-Y. Tournet, and H. Lantéri, “Linear unmixing of hyperspectral images using a scaled gradient method,” in *Proc. IEEE Workshop Stat. Signal Process. (SSP)*, Cardiff, Wales, UK, Aug. 2009, pp. 729–732.
- [14] W. Karush, “Minima of functions of several variables with inequalities as side constraints,” Ph.D. dissertation, Univ. of Chicago, 1939.
- [15] H. W. Kuhn and A. Tucker, “Nonlinear programming,” in *Proc. 2nd Berkeley Symp.*, U. of California Press, Ed., 1951, pp. 481–492.
- [16] H. Lantéri, M. Roche, and C. Aime, “Penalized maximum likelihood image restoration with positivity constraints – multiplicative algorithms,” *Inverse problems*, vol. 18, no. 5, pp. 1397–1419, 2002.
- [17] M. E. Daube-Witherspoon and G. Muehllehner, “An iterative image space reconstruction algorithm suitable for volume ECT,” *IEEE Trans. Medical Imaging*, vol. 5, no. 2, pp. 61–66, June 1986.
- [18] D. P. Bertsekas, *Non linear programming*. Athena Scientific, 1995.
- [19] C.-I Chang, X.-L. Zhao, M. L. G. Althouse, and J. J. Pan, “Least squares subspace projection approach to mixed pixel

- classification for hyperspectral images,” *IEEE Trans. Geosci. and Remote Sensing*, vol. 36, no. 3, pp. 898–912, May 1998.
- [20] D. Manolakis, C. Siracusa, and G. Shaw, “Hyperspectral subpixel target detection using the linear mixing model,” *IEEE Trans. Geosci. and Remote Sensing*, vol. 39, no. 7, pp. 1392–1409, July 2001.
- [21] J. Wang and C.-I Chang, “Applications of independent component analysis in endmember extraction and abundance quantification for hyperspectral imagery,” *IEEE Trans. Geosci. and Remote Sensing*, vol. 44, no. 9, pp. 2601–2616, Sept. 2006.
- [22] C. L. Lawson and R. J. Hanson, *Solving Least Squares Problems*. Prentice-Hall, 1974.
- [23] RSI (Research Systems Inc.), *ENVI User’s guide Version 4.0*, Boulder, CO 80301 USA, Sept. 2003.
- [24] R. N. Clark, G. A. Swayze, and A. Gallagher, “Mapping minerals with imaging spectroscopy, U.S. Geological Survey,” *Office of Mineral Resources Bulletin*, vol. 2039, pp. 141–150, 1993.
- [25] R. N. Clark *et al.*, “Imaging spectroscopy: Earth and planetary remote sensing with the USGS Tetracorder and expert systems,” *J. Geophys. Res.*, vol. 108, no. E12, pp. 5–1–5–44, Dec. 2003.
- [26] I. Dópido, A. Villa, A. Plaza, and P. Gamba, “A quantitative and comparative assessment of unmixing-based feature extraction techniques for hyperspectral image classification,” *IEEE J. Sel. Topics Applied Earth Observations and Remote Sens.*, vol. 5, no. 2, pp. 421–435, 2012.
- [27] J. Bioucas-Dias and M. A. T. Figueiredo, “Alternating direction algorithms for constrained sparse regression: Application to hyperspectral unmixing,” in *Proc. IEEE GRSS Workshop Hyperspectral Image Signal Process.: Evolution in Remote Sens. (WHISPERS)*, 2010, pp. 1–4.
- [28] C.-W. Hsu and C.-J. Lin, “A comparison of methods for multiclass support vector machines,” *IEEE Trans. Neur. Net.*, vol. 13, no. 2, pp. 415–425, 2002.
- [29] J. Llacer and J. Nuñez, “Iterative maximum likelihood and Bayesian algorithms for image reconstruction in astronomy,” in *The restoration Of Hubble Space Telescope images*, R. L. White and R. J. Allen, Eds. The Space Telescope Science Institute, 1990, pp. 62–69.
- [30] T. S. Zacheo and R. A. Gonsalves, “Iterative maximum-likelihood estimators for positively constrained objects,” *J. Opt. Soc. Am. A*, vol. 13, no. 2, pp. 236–242, Feb 1996.